D. Vimercati, G. Gori, A. Spinelli, A. Guardone
*Non-Ideal Effects on the Typical Trailing Edge Shock Pattern of Orc Turbine Blades*
Energy Procedia, Vol. 129, 2017, p. 1109-1116
doi:10.1016/j.egypro.2017.09.231

Available online at www.sciencedirect.com

ScienceDirect

Energy Procedia 129 (2017) 1109–1116

Energy Procedia

www.elsevier.com/locate/procedia

IV International Seminar on ORC Power Systems, ORC2017
13-15 September 2017, Milano, Italy

# Non-ideal effects on the typical trailing edge shock pattern of ORC turbine blades

D.Vimercati[a], G.Gori[a], A.Spinelli[b], A.Guardone[a,*]

[a]*Department of Aerospace Science & Technology, Politecnico di Milano, Via La Masa 35, 20156 Milano, Italy*
[b]*Energy Department, Politecnico di Milano, Via Lambruschini 4, 20156 Milano, Italy*

**Abstract**

At the trailing edge of supersonic high-pressure turbine vanes, a typical shock pattern, the so-called fish-tail shocks, originates due to the flow rotation imposed by its finite thickness. In addition, shock and shock/fan systems can arise in case of a post-expanded channel design or at off-design conditions. ORC turbine stator blades are particularly prone to this phenomena since they are designed to provide a high outlet Mach number, especially at the first stage. In the close proximity of the saturation curve, near the critical point, molecularly complex organic fluids for ORC applications may exhibit a number of non-ideal gasdynamic effects, including a remarkable dependency of the shock properties on the upstream thermodynamic state of the fluid, at a fixed upstream Mach number. The influence of thermodynamic conditions on the shock pattern is assessed as a function of the flow deviation and compared against the ideal gas case, for which the shock properties depends on the upstream Mach number only. Non-ideal effects are investigated here using siloxane vapor MDM (Octamethyltrisiloxane, $C_8H_{24}O_2Si_3$), as an exemplary organic fluid. The present results can be arguably extended to most vapors currently employed in ORC applications.


Peer-review under responsibility of the scientific committee of the IV International Seminar on ORC Power Systems.

*Keywords:* Non-ideal Compressible-Fluid Dynamics, Supersonic flows, Siloxane fluid MDM, SU2, Fish-tail shock waves, Non-ideal oblique shock waves, ORC applications

## 1. Introduction

In the recent past, Organic Rankine Cycle (ORC) systems received a growing interest owing to their good performances and flexibility in the conversion of thermal power coming from low to medium temperature heat sources, such as industrial waste heat, geothermal reservoirs and biomass combustion. In order to meet design and performance requirements, the working fluids employed in ORCs are molecularly complex fluids, typically heavy hydrocarbons, fluorocarbons and siloxanes. These substances exhibit strong non-ideal compressible-fluid features in the range of pressures and temperatures of interest for ORC applications. In particular, focusing on the turbine passage, the expansion process occurs in the single-phase vapour region in proximity of the liquid-vapour saturation curve and critical

* Corresponding author.
*E-mail address:* alberto.guardone@polimi.it

1876-6102 
Peer-review under responsibility of the scientific committee of the IV International Seminar on ORC Power Systems.
10.1016/j.egypro.2017.09.231

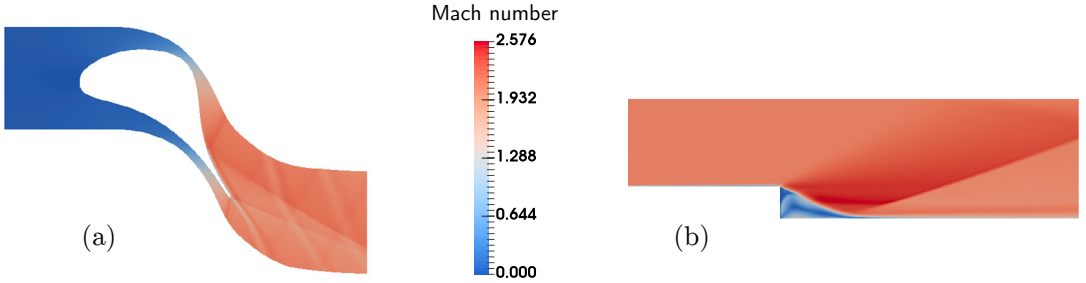


Fig. 1. Predicted time-averaged Mach number field of siloxane MDM by RANS calculations using the non-ideal solver from the SU2 suite. (a) Flow within a typical ORC turbine vane, details on the geometry can be found in Ref. [1, 2]. Total upstream conditions $P^t$ = 8 bar, $T^t$ = 272 °C; (b) Flow over a backward facing step. Static upstream conditions $P$ = 1 bar, $T$ = 242 °C, $M$ = 2;

point, where the fluid experiences non-ideal compressibility effects primarily related to the peculiar behaviour of the speed of sound. To this extent, a deep understanding of the non-ideal compressible-fluid dynamics (NICFD) is of utmost importance for the improvement of ORC system performances and justifies the ongoing research and development in this relatively recent branch of fluid mechanics.

One of the drawbacks of utilizing complex organic vapours lies in the low values of the speed of sound characterizing the thermodynamic conditions typical of ORC expanders. This causes the flow to easily reach high flow Mach numbers at the nozzle exit, especially for the initial stages (particularly the first stage) due to the relatively large pressure ratios. The supersonic stream at the trailing edge of the stator vanes may possibly result in large losses, making the trailing-edge region critical to turbine efficiency [3, 4]. The flow pattern at a supersonic trailing edge is well understood [5] and potentially comprises different wave systems (e.g. shock/shock, shock/Prandtl-Meyer fan) either at design or off-design conditions. A typical shock pattern, the so-called fish-tail shocks, always originates at the trailing edge, due to the flow rotation imposed by its finite thickness. Also, a flow deviation from the geometrical blade angle can be required in the case of a post-expanded channel design. Even in the theoretical case of infinitesimal trailing edge thickness, the post-expansion achieved by the deviation occurs through an oblique shock/Prandtl-Meyer fan system on the blade suction and pressure side, respectively. These features are shown in Fig. 1a, where the time-averaged Mach number field is depicted for an exemplary ORC turbine vane. The flow-field around the blade is computed using the SU2 [6] non-ideal solver [7]. Simulation were carried out using the iPRSV EOS [8] to model the thermodynamic behavior of the working fluid. Note that from the qualitative standpoint the trailing edge flow configuration is similar to the one occurring in a supersonic flow over a backward facing step, see Fig. 1b. Here, a supersonic Prandtl-Meyer expansion occurs and a limited region of separation is generated behind the step. At the end of the separation bubble, compressive waves coalesce into an oblique shock wave.

Since the trailing edge thickness is always of finite dimension, both the flow rotation at the trailing edge and the downstream flow deviation contribute to define the trailing edge shock pattern. The formation of shock represents itself a source of losses and further losses are typically induced from shock-boundary layer interactions at the adjacent blades. Moreover, periodical mechanical stresses arise at rotor blades interacting with upstream shocks, which can be of relevant strength, especially at off-design conditions. ORC turbine stator blades are particularly prone to this phenomena, since they are designed to provide high outlet Mach number, especially at the first stage. Recent investigations [9, 10] pointed out the influence of the fundamental derivative of gasdynamics $\Gamma$ [11] (see Eq. 3) on the flow pattern downstream of typical ORC vane trailing edge, by comparing working fluids with increasing complexity. A reduction of the separated region is observed at decreasing values of $\Gamma$, associated with the larger turning angles that the flow sustains across Prandtl-Meyer waves. The shape and extension of the separated region downstream the trailing edge largely affects the subsequent fish-tail shock structure, which can possibly be required to deliver large flow angles deflections in order to match the flows from the suction and pressure blade surfaces. Both the fluid molecular complexity and non-ideal flow effects influence the separation pattern, thus the features of oblique shocks originating from it.

The present work aims at investigating the possible non-ideal effects across oblique shock waves and the influence of thermodynamic conditions on the shock properties. For a given flow deviation, the shock configuration is influ-

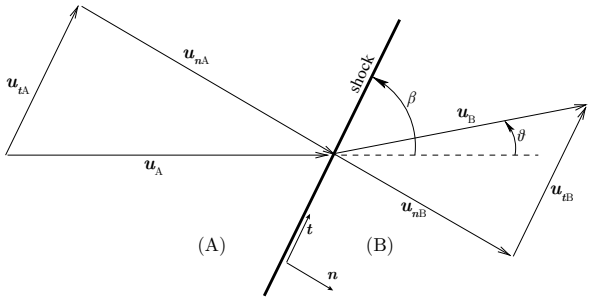


Fig. 2. Qualitative illustration of the local shock front. For ease of representation, a two-dimensional configuration is sketched. States A and B represent the pre-shock and post-shock states, respectively, $\boldsymbol{u}$ is the fluid velocity for an observer moving with the shock wave and $u_{\boldsymbol{n}}$ and $\boldsymbol{u}_{\boldsymbol{t}}$ denote the normal and parallel velocity components with respect to the shock front. The angles $\beta$ and $\theta$ are the shock angle and flow deviation angle, both computed with respect to the pre-shock flow direction.

enced by the upstream (pre-shock) Mach number and thermodynamic state. This contrasts the perfect-gas case, for which the upstream Mach number determines the shock configuration and the upstream thermodynamic conditions are not relevant. The influence of the upstream thermodynamic state on the shock properties is shown to be not only quantitative (e.g. shock angle for a given deviation), but and also qualitative (the Mach number can possibly increase across the oblique shock, see Ref. [12]). The present analysis is carried out for siloxane vapor MDM (Octamethyltrisiloxane, $C_8H_{24}O_2Si_3$), by considering exemplary flow configurations. Nonetheless, the same non-ideal behaviour observed for MDM is expected also for different fluids of interest for ORC applications, as molecularly complex vapours exhibit the same qualitative behaviour in the close proximity of the saturation curve [13, 14].

The present work is organised as follows: in section 2, the jump relations across surfaces of discontinuity are recalled together with the computation of polar diagrams. In section 3, relevant non-ideal effects across oblique shock waves are discussed with reference to siloxane MDM. Section 4 presents the concluding remarks.

## 2. Methodology

Shock waves are discontinuous solutions to the Euler equations of gasdynamics, namely the governing equations for inviscid non-heat-conducting fluid flows. The balance of mass, momentum and energy across the surface of discontinuity are expressed by the well-known Rankine-Hugoniot relations, see, e.g., Ref. [15]. With reference to Fig. 2, the Rankine-Hugoniot relations for two-dimensional flows locally assume the form

$$\begin{aligned} [h] &= \tfrac{1}{2}[P](v_\mathrm{A} + v_\mathrm{B}), \\ -[P]/[v] &= (\rho_\mathrm{A}\|\boldsymbol{u}_\mathrm{A}\|\sin\beta)^2, \\ \rho_\mathrm{A}\tan\beta &= \rho_\mathrm{B}\tan(\beta-\vartheta), \\ \|\boldsymbol{u}_\mathrm{A}\|\cos\beta &= \|\boldsymbol{u}_\mathrm{B}\|\cos(\beta-\vartheta), \end{aligned} \tag{1}$$

where subscripts A and B indicate the upstream (pre-shock) and downstream (post-shock) quantities, respectively, and $[\cdot] = ()_\mathrm{B} - ()_\mathrm{A}$ the corresponding jump across the discontinuity. In the above expressions, $P$ is the pressure, $v$ is the specific volume, $\rho = 1/v$ is the density, $h$ is the specific enthalpy, $\boldsymbol{u}$ is the fluid velocity in a reference frame moving with the shock wave and finally $\beta$ and $\theta$ denote the angle of the shock wave with respect to the upstream flow direction and the flow deviation, respectively. In particular, one can recognize the Hugoniot relation (Eq. 1a), which determines the locus of thermodynamic states that can be connected by a shock wave, and the equation of the Rayleigh line (Eq. 1b), the straight line in $P$–$v$ plane connecting the pre-shock and post-shock states. Moreover, Eq. 1d implies that the tangential velocity is conserved across the shock front, so that the oblique shock problem can be reduced to that of a normal shock to which a parallel velocity field is superposed. Among the solutions of Sys. 1, those which are physically admissible must satisfy the entropy condition

$$[s] > 0, \tag{2}$$

where $s$ denotes the specific entropy. We will restrict our attention to fluids exhibiting positive nonlinearities, namely, we assume that the fundamental derivative of gasdynamics $\Gamma$ [11] is positive,

$$\Gamma = 1 + \rho c \left(\frac{\partial c}{\partial P}\right)_s = \frac{v^3}{2c^2}\left(\frac{\partial^2 P}{\partial^2 v}\right)_s > 0. \tag{3}$$

The fundamental derivative is a non-dimensional measure of the isentropic speed of sound variation with pressure or, equivalently, of the curvature of isentropes in the $P$–$v$ plane. In the context of classical gasdynamics dealing with positive-$\Gamma$ fluids, the requirement that entropy not decrease across the shock wave is sufficient to isolate physically realizable shock solutions, see Ref. [16], and implies the well-known result that only compressive shocks, i.e. $[P] > 0$, are admissible.

A comprehensive description of the properties of oblique shock waves is provided by the so-called polar curves, which will be extensively used in the following section and are briefly recalled here. Diagrams reporting the values of post-shock quantities, or the shock angle as well, as a function of the deflection angle are known as deflection shock polars. For instance, the $(P_\mathrm{B}, \vartheta)$–polar is the pressure–deflection polar and the $(\beta, \vartheta)$–polar is the shock angle–deflection polar. If the pre-shock state A and the deviation angle $\vartheta$ are fixed, then, taking into account the equation of state $h = h(P, v)$, Eq. 1 can be solved for the unknowns $(P_\mathrm{B}, v_\mathrm{B}, \boldsymbol{u}_\mathrm{B}, \beta)$, provided that the deviation angle does not exceed a maximum value $\vartheta_\mathrm{max}$, which depends on the pre-shock state. For $\vartheta < \vartheta_\mathrm{max}$, Eq. 1 yields two different solutions, namely the strong oblique shock (larger shock angle and pressure jump, downstream flow is always subsonic) and the weak oblique shock (lower shock angle and pressure jump, downstream flow always supersonic with the exception of a small interval in the close proximity of $\vartheta_\mathrm{max}$). Note, in particular, that $\vartheta = 0$ yields the trivial shock, namely, $\beta = \sin^{-1}(1/M_\mathrm{A})$, the acoustic angle, where $M = \|\boldsymbol{u}\|/c$ is the flow Mach number, and the normal shock solution.

## 3. Non-ideal effects across oblique shock waves in typical ORC turbine operation

In the present section, relevant non-ideal effects on the properties of oblique shock waves are discussed by analysing the shape of selected shock polars for siloxane MDM, modelled using the state-of-the-art EOS available from the REFPROP library [17]. The possibility to extend the following results to other fluids is addressed in the concluding remarks.

Most of the properties of oblique shock waves in a perfect gas, including e.g. the shock angle–deviation polar, the Mach number–deviation polar and the deviation polar of the static pressure ratio, depend uniquely on the upstream flow Mach number $M_\mathrm{A}$, see for instance Ref. [18]. On the contrary, when a non-ideal equation of state is used to compute the thermodynamic properties of the fluid, a more or less noticeable dependence on the upstream thermodynamic state, say the upstream values of temperature and pressure, is also observed.

In the following, two parametric studies are conducted to assess the shock polar dependence on the upstream thermodynamic state for a fixed upstream Mach number ($M_\mathrm{A} = 2$ and $M_\mathrm{A} = 1.5$ in the first and second study, respectively). For both studies, the upstream entropy is fixed ($s_\mathrm{A} = s(0.557P_c, 0.964T_c)$, corresponding to the inlet entropy of the stator passage shown in Fig. 1a. Different upstream pressures are considered. The range in which the upstream thermodynamic state is allowed to vary corresponds to the thermodynamic region close to the saturation curve and critical point, namely in the typical region of operation of ORC turbines. The thermodynamic region of interest here, see Fig. 3, is characterized by values of the fundamental derivative $\Gamma$ lower than unity, which implies that the speed of sound decreases upon isentropic compression. Several non-ideal effects are related to the condition $\Gamma < 1$, see e.g. Ref. [11, 19, 20]. These phenomena also affect the shape of the shock polars, as it is shown below.

The first parametric study, carried out for $M_\mathrm{A} = 2$ and a pressure range $P_\mathrm{A}/P_c \in [0.070, 0.557]$ along the reference isentrope, is shown in Fig. 4a-d. Figure 4a shows the shock angle–deviation polars obtained from the reference EOS implemented in REFPROP (blue lines) and from the perfect gas model of MDM (red line). For the reference EOS, significant modifications to the shock angle–deviation polar are observed for different values of the upstream pressure. In particular, in the acoustic limit $\vartheta \to 0$ and $[P] \to 0$, the dependence on the upstream thermodynamic state can be explicitly evaluated thanks to the Taylor series expansion:

$$\beta = \sin^{-1}(1/M_\mathrm{A}) + \frac{\Gamma_\mathrm{A}}{2}\frac{M_\mathrm{A}^2}{M_\mathrm{A}^2 - 1}\vartheta + O(\vartheta^2), \qquad \vartheta \to 0 \text{ and } [P] \to 0. \tag{4}$$

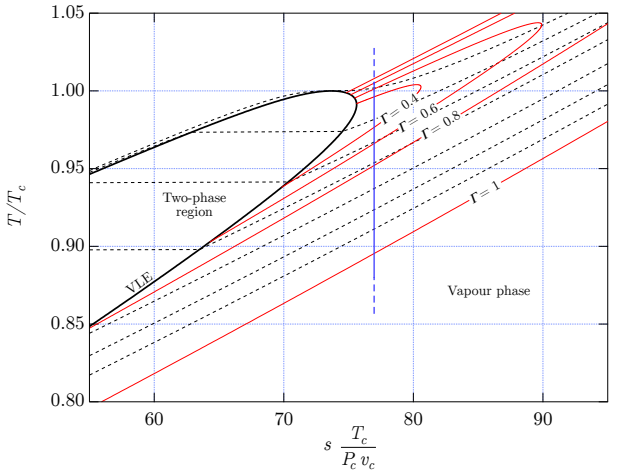


Fig. 3. Temperature–entropy diagram for MDM, computed from the reference EOS [17], showing the selected isentrope (blue line) for the parametric studies, $s_A = s(0.557P_c, 0.964T_c)$. Also shown is a set of isobars (black dashed lines) and Γ–contours (red lines).

Besides the dependence on $M_A$, which holds also in the perfect gas case, the above expression points out the dependence on the upstream thermodynamic state, rooted for any non-ideal EOS in the parameter $\Gamma_A$. With reference to Fig. 3, the range of the selected upstream thermodynamic states is such that $\Gamma_A$ increases with $P_A$, thus justifying the shock polar configurations observed in Fig. 4a. In addition to the shock behaviour in the acoustic limit, another significant non-ideal effect is related to the maximum deviation angle that the flow can sustain. As depicted in Fig. 4a, and more in detail in Fig. 4b, the maximum deviation $\vartheta_{max}$ can possibly attain much larger values in the non-ideal regime than in dilute conditions. Also, note in Fig. 4b a non-monotonic dependence of $\vartheta_{max}$ on $P_A$ along the selected isentrope. The Mach–deviation polars, see Fig. 4c, reveal that non-ideal effects are not only quantitative, but also qualitative, inasmuch as the Mach number can possibly increase, rather than decrease, across an oblique shock wave. This phenomenon, which is due to the non-monotonic variation of the speed of sound along the shock adiabat, is possible only in fluid exhibiting $\Gamma < 1$, see Ref. [12]. Shock waves with $M_B > M_A$ are called non-ideal oblique shock waves in the following. The acoustic limit makes it possible to explicitly ascertain the influence of the upstream state on the downstream Mach number. The Taylor series expansion of the downstream Mach number, in the acoustic limit, assumes the form

$$M_B = M_A + \frac{J_A M_A^3}{\sqrt{M_A^2 - 1}}\vartheta + O(\vartheta^2), \qquad \vartheta \to 0 \text{ and } [P] \to 0, \tag{5}$$

having defined $J = 1 - \Gamma - 1/M^2$ [21] and showing, once again, the dependence on the upstream thermodynamic state through Γ only. Note that, in order to observe a Mach number increase across an oblique shock wave of small strength, the upstream Mach number must be sufficiently large, so that $J_A > 0$. The latter relation is a sufficient condition for the Mach number to increase across oblique shocks. It is also possible, for oblique shocks of larger strength, that the Mach number increases across the shock despite $J_A < 0$, as shown in Fig. 4c for $P_A/P_c = 0.345$. Finally, Fig. 4d shows the deviation polar of the total pressure ratio, which allows to account for the loss across the oblique shock wave. Both the weak and strong oblique shock branches exhibit non-monotonic properties in the range of pressures considered. If, for instance, the flow deviation $\vartheta$ is fixed, the total pressure loss initially increases with the upstream pressure, but eventually decreases for the largest pressure values considered.

A similar parametric study has been carried out for $M_A = 1.5$ and is shown in Fig. 5a-d. Here, the pressure range $P_A/P_c \in [0.070, 0.696]$ is considered along the reference isentrope. The oblique shock configurations of Fig. 5a-d show the same trends observed in the previous parametric study for $M_A = 2$. Further computations performed for different upstream Mach numbers (not shown here) confirm the present findings. Note that there exist a minimum value of the upstream Mach number, namely $M_{A,min} = (1 - \Gamma_{min})^{-1/2}$ where $\Gamma_{min}$ is the minimum value of the fundamental

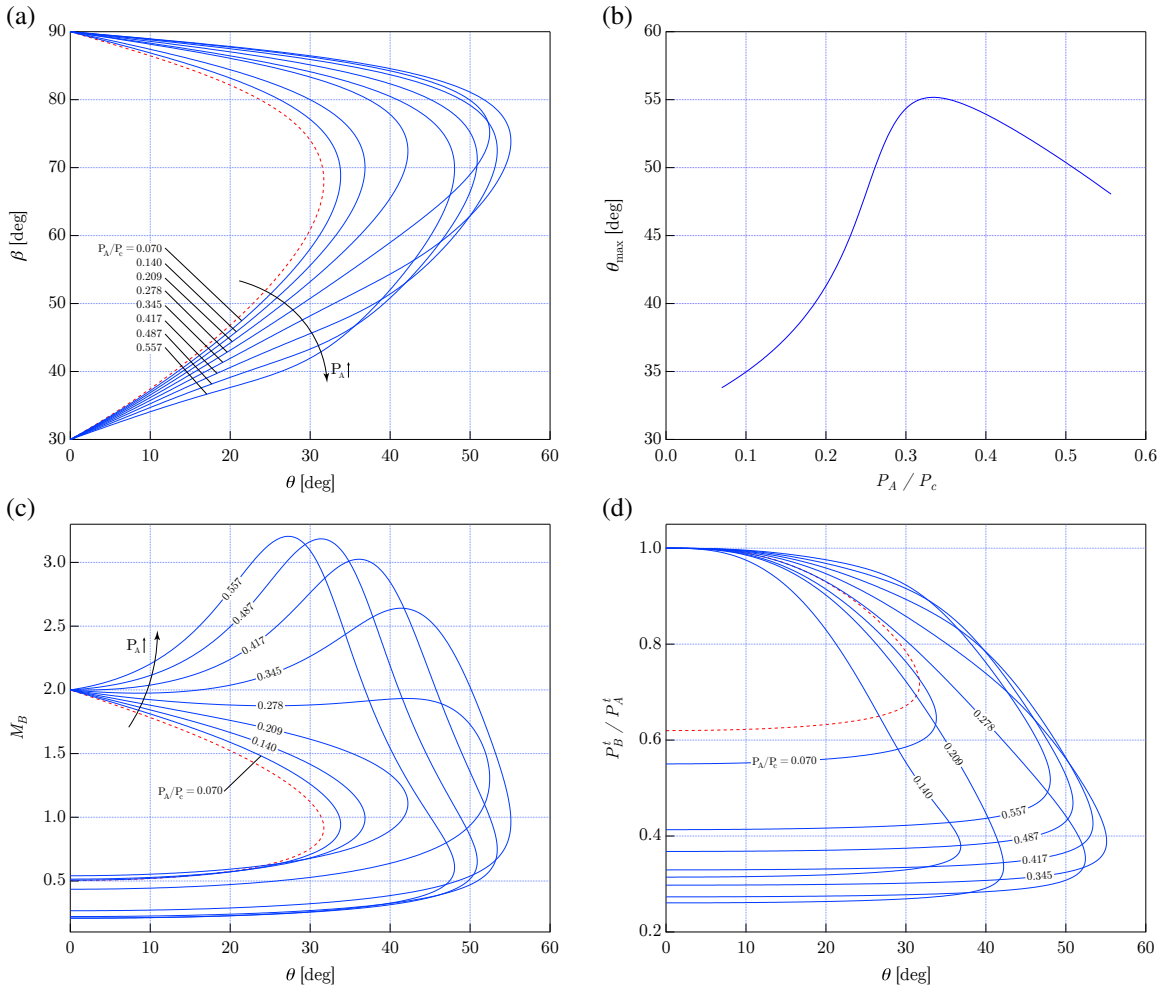


Fig. 4. Shock polars (blue) for MDM, computed from the reference EOS [17]. The upstream Mach number and entropy are fixed to $M_A = 2$ and $s_A = s(0.557P_c, 0.964T_c)$, respectively; the considered pressure range is $P_A/P_c \in [0.070, 0.557]$. (a) Shock angle–deviation polar; (b) Variation of the maximum deviation angle with the upstream pressure; (c) Mach number–deviation polar; (d) Total pressure ratio–deviation polar. Also shown (red dashed line) are the polars obtained from the perfect gas model of MDM.

derivative in the vapour phase, for which the downstream Mach number can increase across oblique of small strength (i.e. in the acoustic limit).

## 4. Conclusions

Oblique shock waves in the non-ideal regime of siloxane MDM were investigated within thermodynamic regions typical of ORC turbine operation. Differently from the perfect gas case, the upstream thermodynamic state was found to play a major role in determining the variation of relevant properties across the shock. In particular, these include the maximum flow deflection angle, the Mach number variation and the total pressure loss across the shock. In addition, in the acoustic limit it was found that the variation of the shock angle and of the downstream Mach number with the flow deflection ultimately depend on the upstream value of the fundamental derivative of gasdynamics.

The non-ideal effects investigated in this work are of utmost importance for ORC turbomachinery applications, since shock waves generated at the trailing edge of supersonic stator blades largely affect the overall stage performances. In this respect, the understanding of the main parameters of influence on the characteristic shock wave pattern is key to improve the correct estimation of losses. Despite the present study is limited to siloxane MDM

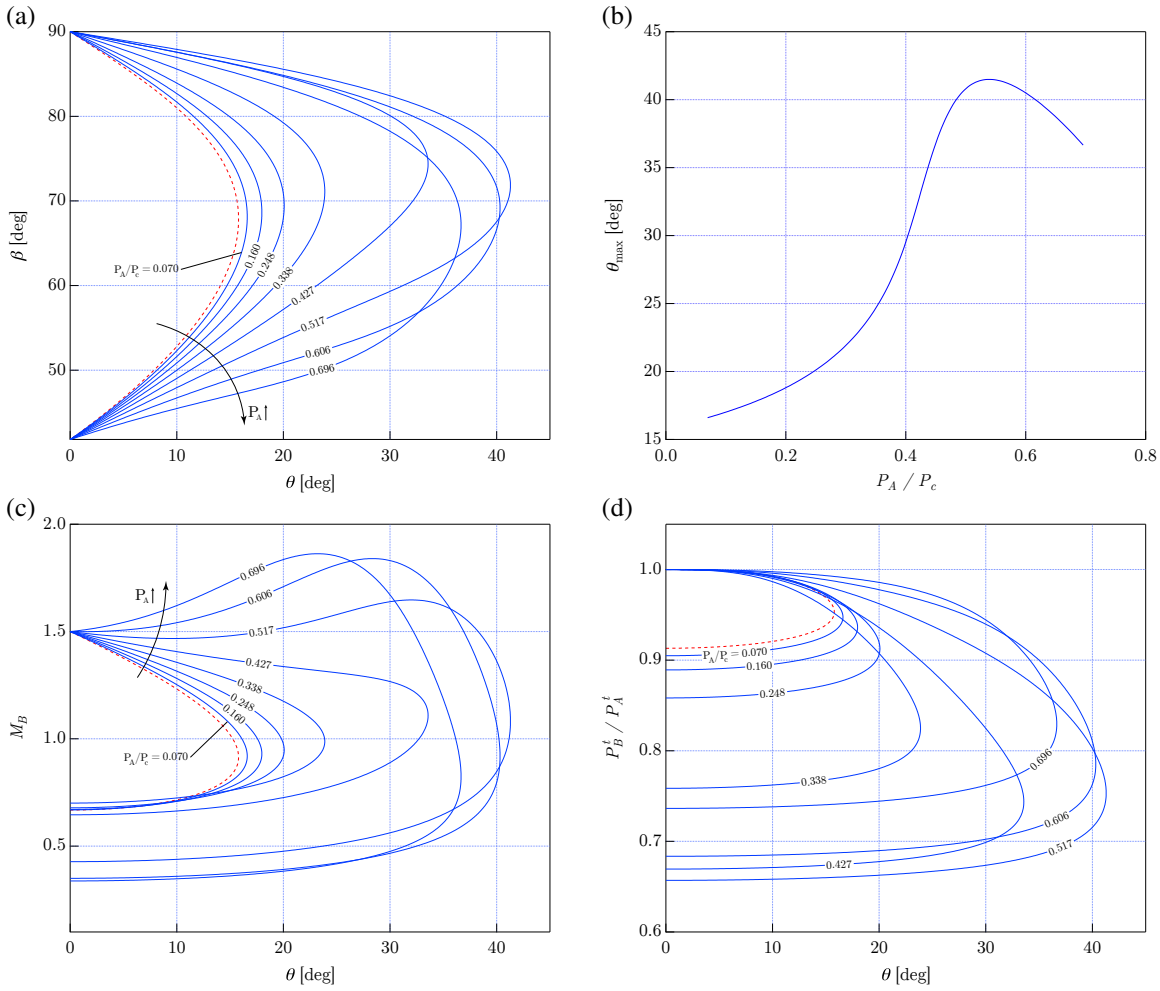


Fig. 5. Same as Fig. 4, but with $M_{\mathrm{A}} = 1.5$ and $P_{\mathrm{A}}/P_c \in [0.070, 0.696]$.

only, most moderate-to-high molecularly complex fluids exhibit the same qualitative behaviour, in accordance with the principle of corresponding states, and therefore the present analysis arguably apply to several different fluids employed in ORC power systems. This is confirmed by the calculations shown in Fig. 6. In Fig. 6(left), the variation of the fundamental derivative along the isentrope tangent to the saturated vapour boundary (local entropy maximum which occurs in retrograde fluids) is plotted for different ORC working fluids, showing the same qualitative trends. Moreover, Fig. 6(right) reports the minimum values of the total pressure and temperature leading to $J \geq 0$, and thus to the possibility of observing Mach number–increasing (weak) oblique shocks, along the same isentrope. These values would correspond to supercritical ORCs and are within the thermal stability limit for isopentane and R245fa, closer to the limit for MM, toluene and cyclopentane, while they appear to be slightly above the limit for MDM.

## Acknowledgements

The research is partially funded by the European Research Council under Grant ERC Consolidator 2013, project NSHOCK 617603.

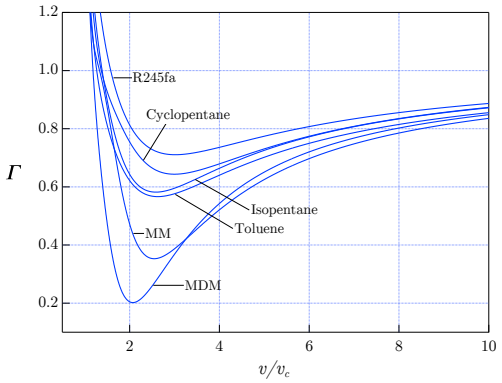


| Fluid | $P^t_{\min}/P_c$ | $T^t_{\min}/T_c$ |
|---|---|---|
| MDM | 1.174 | 1.015 |
| MM | 1.335 | 1.031 |
| Toluene | 1.808 | 1.061 |
| Isopentane | 1.918 | 1.073 |
| Cyclopentane | 2.129 | 1.082 |
| R245fa | 2.952 | 1.117 |

Fig. 6. Results for different fluids currently employed in ORC power systems. Left: variation of the fundamental derivative with the specific volume, along the isentrope tangent to the saturation curve; right: minimum total pressure and temperature values for $J \geq 0$ along the isentrope tangent to the saturation curve. Reference thermodynamic models from the REFPROP library [17].

## References


[1] Colonna, P., Harinck, J., Rebay, S., Guardone, A.. Real-gas effects in Organic Rankine Cycle turbine nozzles. J Propul Power 2008;24(2):282–294.

[2] Pini, M., Persico, G., Pasquale, D., Rebay, S.. Adjoint method for shape optimization in real-gas flow applications. Journal of Engineering for Gas Turbines and Power 2015;137(3).

[3] Denton, J., Xu, L.. The trailing edge loss of transonic turbine blades. In: ASME 1989 International Gas Turbine and Aeroengine Congress and Exposition. 1989,.

[4] Mee, D., Baines, N., Oldfield, M., Dickens, T.. An examination of the contributions to loss on a transonic turbine blade in cascade. In: ASME 1990 International Gas Turbine and Aeroengine Congress and Exposition. 1990,.

[5] Saracoglu, B., Paniagua, G., Sanchez, J., Rambaud, P.. Effects of blunt trailing edge flow discharge in supersonic regime. Computers & Fluids 2013;88:200–209.

[6] Palacios, F., Alonso, J., Duraisamy, K., Colonno, M., Hicken, J., Aranake, A., et al. Stanford University Unstructured (SU 2): an open-source integrated computational environment for multi-physics simulation and design. In: 51st AIAA Aerospace Sciences Meeting Including the New Horizons Forum and Aerospace Exposition. 2013, p. 287.

[7] Vitale, S., Gori, G., Pini, M., Guardone, A., Economon, T.D., Palacios, F., et al. Extension of the SU2 open source CFD code to the simulation of turbulent flows of fuids modelled with complex thermophysical laws. In: 22nd AIAA Computational Fluid Dynamics Conference. 2015, p. 2760.

[8] Stryjek, R., Vera, J.H.. PRSV: An improved Peng-Robinson equation of state for pure compounds and mixtures. Can J Chem Eng 1986;64:323–333.

[9] Galiana, F.J.D., Wheeler, A.P., Ong, J.. A study of trailing-edge losses in organic rankine cycle turbines. Journal of Turbomachinery 2016;138(12):121003.

[10] Galiana, F.D., Wheeler, A., Ong, J., de M Ventura, C.. The effect of dense gas dynamics on loss in orc transonic turbines. In: Journal of Physics: Conference Series; vol. 821. IOP Publishing; 2017, p. 012021.

[11] Thompson, P.A.. A fundamental derivative in gasdynamics. Phys Fluids 1971;14(9):1843–1849.

[12] Gori, G., Vimercati, D., Guardone, A.. Non-ideal compressible-fluid effects in oblique shock waves. In: Journal of Physics: Conference Series; vol. 821. IOP Publishing; 2017, p. 012003.

[13] Harinck, J., Guardone, A., Colonna, P.. The influence of molecular complexity on expanding flows of ideal and dense gases. Phys Fluids 2009;21(8):086101.

[14] Colonna, P., Guardone, A., Nannan, R., van der Stelt, T.P.. On the computation of the fundamental derivative of gas dynamics Γ using equations of state. Fluid Phase Equilib 2008;.

[15] Hayes, W.D.. The basic theory of gasdynamic discontinuities. In: Emmons, H.W., editor. Fundamentals of gasdynamics; vol. 3 of *High speed aerodynamics and jet propulsion*. Princeton, N.J.: Princeton University Press; 1958, p. 416–481.

[16] Menikoff, R., Plohr, B.J.. The Riemann problem for fluid flow of real material. Rev Mod Phys 1989;61(1):75–130.

[17] Lemmon, E.W., Huber, M.L., McLinden, M.O.. NIST reference database 23: reference fluid thermodynamic and transport properties–REFPROP, version 9.1. Standard Reference Data Program 2013;.

[18] Thompson, P.A.. Compressilbe Fluid Dynamics. McGraw-Hill; 1988.

[19] Cramer, M.S., Kluwick, A.. On the propagation of waves exhibiting both positive and negative nonlinearity. J Fluid Mech 1984;142:9–37.

[20] Cramer, M.S., Best, L.M.. Steady, isentropic flows of dense gases. Phys Fluids A 1991;3(4):219–226.

[21] Cramer, M.S., Crickenberger, A.B.. Prandtl-Meyer function for dense gases. AIAA Journal 1992;30(2):561–564.